JOURNAL OF THERMOPHYSICS AND HEAT TRANSFER
Vol. 20, No. 1, January–March 2006

Kinetic Model of Condensation in a Free Argon Expanding Jet

Jiaqiang Zhong,* Michael I. Zeifman,† and Deborah A. Levin‡
Pennsylvania State University, University Park, Pennsylvania 16802

The direct-simulation Monte Carlo (DSMC) method has recently been developed to simulate homogeneous condensation in a free-expansion rocket plume. However, cluster–monomer and cluster–cluster collision models as well as the determination of cluster size were simplified in the previous work, and the effect on the accuracy of the numerical simulation results was not quantified. In this work, the molecular-dynamics (MD) method is used to simulate collision and sticking probabilities for argon clusters and the results are compared with the hard-sphere model. These improved models are then integrated into a DSMC code to predict the Rayleigh scattering intensity in a free-expanding argon condensation plume, and numerical results are compared with experimental data along the plume centerline.

Nomenclature

A = constant
B = constant
b = impact parameter
c = velocity
d = diameter
E = evaporation rate or energy
I = intensity
i = number of atoms
J = nucleation rate
K = intensity constant
k_B = Boltzmann's constant
L = specific latent heat
M = cluster mass
m = molecular mass
N = number density
n_c = number of simulated nuclei particles
p_s = saturation pressure
q = sticking coefficient
R = ideal gas constant
r = distance or radius
T = temperature
V = interaction potential or specific volume
α = species polarizability
Δt = time step
ΔV = cell volume
ϵ = potential constant
λ_0 = wavelength
ρ = density
σ = surface tension or potential constant

Subscripts

c = cluster species
i = cluster size
ref = reference value
v = vapor state
$*$ = critical state

Presented as Paper 2005-0767 at the AIAA 43rd Aerospace Science Meeting, Reno, NV, 10–13 January 2005; received 2 February 2005; revision received 13 May 2005; accepted for publication 14 May 2005.

*Graduate Student, Department of Aerospace Engineering. Student Member AIAA.
†Research Associate, Department of Aerospace Engineering. Member AIAA.
‡Associate Professor, Department of Aerospace Engineering. Associate Fellow AIAA.

I. Introduction

HOMOGENEOUS condensation,[1] observed in various types of plumes expanding into a vacuum, may result in contamination of spacecraft surfaces as well as affect the observance of high-altitude plumes.[2,3] Extensive experimental studies on the condensation in real thrusters and small free-expanding jets have been conducted since the 1970s.[4,5] However, it is difficult to measure cluster-size and number-density distributions in an operational plume. Therefore, a prediction tool that can be validated with small thruster data would provide crucial information about homogeneous condensation in typical chemical-rocket plumes.

Most of the numerical work on condensation coupled to gas expansion models the processes in ground-based facilities and uses continuum approaches.[6] Because free-expanding jets are mostly in the transitional to rarefied regimes, a continuum approach would not simulate condensation for such plumes. Thus, a more appropriate approach that incorporates transitional effects should be used. Such an approach must address the processes of cluster nucleation, growth, and decay, and collisions with other clusters and monomers as well as the usual gas kinetics and is, therefore, computationally challenging.

Recently, the direct simulation Monte Carlo (DSMC)[7] method has been applied to simulate homogeneous condensation in free-expansion plumes.[8,9] The previous work[8] can be summarized as follows. Classical nucleation theory (CNT)[1] was used to model the generation of initial nuclei, which are assumed to be created at local critical conditions. Microscopic models, consistent with CNT theory, have been developed from general conservation equations to model sticking and nonsticking collisions, as well as evaporation processes. These models were then integrated into the DSMC method to simulate condensation coupled flow. The DSMC condensation model developed was numerically validated by comparing the simulation results with analytical solutions in one-dimensional test cases, validated by comparison with Hagana's scaling laws,[4] and applied to predict homogeneous condensation in a rocket plume.

In the previous work,[8] clusters were modeled as hard spheres, with radius proportional to $i^{(1/3)}$, where i is the number of molecules in the cluster. The probability of a sticking collision between a cluster and a condensible monomer was simply assumed to be unity[8] or 0.1[9] without validation. Cluster–cluster collisions were assumed to be elastic without any allowance for coalescence, although it was shown that for cases considered in Ref. 8 the number of cluster–cluster collisions was small. The purpose of this work is to improve the fidelity of the models used in the condensation flow by use of the molecular-dynamics (MD) method. MD simulations may be used to test the validity of the model approximations of the previous work.[8]

The MD computational approach has recently been combined with the DSMC method to study multiscale flows. Here we only

mention a few of the papers that have used MD-DSMC hybrid simulation techniques. To model the time evolution process of a plume generated by laser ablation of an organic solid, Zeifman et al.[10] used the MD approach to model the ejection of molecules and clusters from the target and the DSMC approach to model the long-range expansion of the ejected plume. Briehl and Urbassek[11] used a Monte Carlo simulation to model the agglomeration and fragmentation of copper atoms and clusters in an argon gas environment obtained from the DSMC simulation. Recently, Tsuruta and Naka[12] used an MD approach to study the condensation coefficient of water and analyzed one-dimensional condensation flow of water vapor in the presence of a noncondensing gas using the DSMC approach.

The paper is organized as follows. To understand basic cluster model and interactions between a cluster and a molecule, we use the MD[13] approach in Sec. II to simulate cluster–molecule collision and sticking processes. To derive general conclusions from the MD simulations, a 6–12 Lennard–Jones potential, applicable to many species, is used to simulate collision processes between argon clusters and argon monomers. Using reduced units, the MD simulation results of argon species are compared with those of nickel from Ref. 14. In Sec. III, we briefly review the microscopic models developed in our previous work[8] and compare the present, corrected model with the previous models. These models are then used in Sec. IV to simulate a condensation plume in the DSMC method of a free-expanding argon plume through a sonic orifice. Using the DSMC results, the Rayleigh scattering intensity is then calculated and compared with experimental data along the plume centerline.[15]

II. Molecular-Dynamics Simulation

A. Methodology

MD is a computer-simulation technique that allows one to predict the time evolution of a system of interacting particles, for example, atoms or molecules. Each real atom in MD is usually modeled as a point-size particle that interacts with other particles through a defined interaction potential. Once the system initial conditions are defined, in terms of particle coordinates and velocities, the system evolution in time is obtained by solving Hamilton's equations.

The traditional 6–12 Lennard–Jones potential, valid for interactions among many species, is chosen as the interaction potential in this work,

$$V = 4\varepsilon[(\sigma/r)^{12} - (\sigma/r)^{6}] \tag{1}$$

where the potential parameters for argon[16,17] are $\epsilon = 0.0103$ eV and $\sigma = 3.405$ Å.

Trajectories are integrated numerically using the Nordsieck fifth-order predictor–corrector algorithms,[13] which can be summarized as follows. First, new positions as well as time-derivative terms up to the fifth order are predicted at a new time step using a Taylor series expansion. Then, the force acting on each particle is computed for the predicted positions, and error terms are calculated by comparing force terms between the previous and current time steps. Finally, the error terms are used to correct the particle positions and derivatives for the next time step.

B. Initial Clusters

To simulate cluster-collision outcomes using an MD approach, the initial conditions (coordinates and velocities) of each molecule within a cluster must be specified at the start of the simulation. The condition of dimers, obtained from previous modeling of a free-expansion plume,[18] will be used to characterize the initial clusters for the MD simulations discussed in Secs. II.C and II.D.

To explore the physics of the cluster-formation processes in an expanding plume, an MD approach was used to simulate a free argon expansion along the core plume.[18,19] One challenge in the MD modeling of such a system is the selection of a criterion to distinguish clusters, especially dimers, from atoms that are just collision pairs. The Stillinger criterion[20] and a history-tracking approach were used to find stable clusters as follows. First, the collision-duration time between two atoms were simulated by the MD approach for conditions of various impact parameters and relative velocities, and the MD results were compared with Bunker's approximate formula.[21] It was found that the molecular-collision-duration time is usually less than 10^{-11} s. Then, each molecular position in the plume was output every 10^{-11} s during the MD simulation, and a pure geometric Stillinger criterion was used to identify the clusters in the plume. In this way, the observed clusters were tracked using the MD output, that is, every 10^{-11} s until the atoms in the clusters had separated into monomers. We found that the dimer's lifetime could last more than 30 ps in the plume, and they usually originated from a three-atom collision process during which one of the atoms takes away extra energy while the other two form a stable dimer.

To evaluate the cluster cross section and cluster–monomer sticking probabilities, we also need to prepare clusters of size greater than two for cluster configurations, typical of expanding flows. Trimers were created through a dimer–monomer sticking collision, tetramers through trimer–monomer sticking collisions, and so on. To efficiently generate larger clusters, cluster–cluster sticking collisions may be used.

MD simulation results of cluster–monomer collisions are discussed in the Secs. II.C and II.D. Each of the MD simulation results shown in Secs. II.C and II.D are averaged over a large number of the trajectories by randomly rotating the initial cluster around its center of mass.

C. Cluster Model

The cluster–monomer collision process may be used to define the cluster cross section, as the monomer–monomer collision defines molecular cross section in the traditional DSMC approach. To characterize the cluster model, the processes of cluster–monomer collisions are simulated with the MD method, under the condition of various impact parameters b and relative velocities v_{rel}. Sticking collisions are obviously counted as effective collisions; for nonsticking collisions, only trajectories in which the deflection angle is at least 10 deg are counted as collisions. Note that the deflected postcollision particle angle is assumed to be randomly distributed for either the hard-sphere (HS) or variable-hard-sphere (VHS) models in the DSMC simulation.[7] Thus the number of collisions neglected here is less than approximately 3%. The colliding molecules are initially separated sufficiently far from the target cluster such that the effective interaction potential among them is zero.

The collision probability for each case (b, v_{rel}) is defined as the ratio of the number of trajectories that resulted in collisions to the total number of trajectories. For each case, a sample of 200 trajectories is used with the orientation of the target cluster to the randomly chosen monomer. The impact parameter b increases from a head-on collision value of zero to a value in which the cluster–monomer collision probability is close to zero. Relative collision velocities from approximately 150 to 225 m/s are chosen, and the cluster sizes selected for study in the MD simulations range from dimers to 482-mers. The range of cluster size and collision impact parameter are typical in a condensation plume flow.[8] The collision relative velocity corresponds to a translational thermal temperature that is also representative of a typical nondimensional temperature, that is, the ratio of the collision thermal temperature to the species freezing temperature.

Representative MD simulation results are shown in Fig. 1. The collision probability is close to unity for the cases with relatively small impact parameters. For the cluster collision probability of dimer–monomer collisions, for example, it can be seen that for impact parameters b less than $b_s \approx 7.5$ Å, the probability is almost independent of the impact parameter b. For collisions with b greater than b_s, the collision probability decreases rapidly to zero as the impact parameter increases. It can also be seen that b_s, defined as the critical impact parameter, increases as the cluster size increases.

The maximum impact parameter b_m, chosen here to correspond to a collision probability of 0.1, can be used to calculate the cluster–monomer collision cross section σ as $\sigma = \pi b_m^2$. It is related to the cluster and monomer diameters as[7]

$$b_m = (d_c + d_0)/2 \tag{2}$$

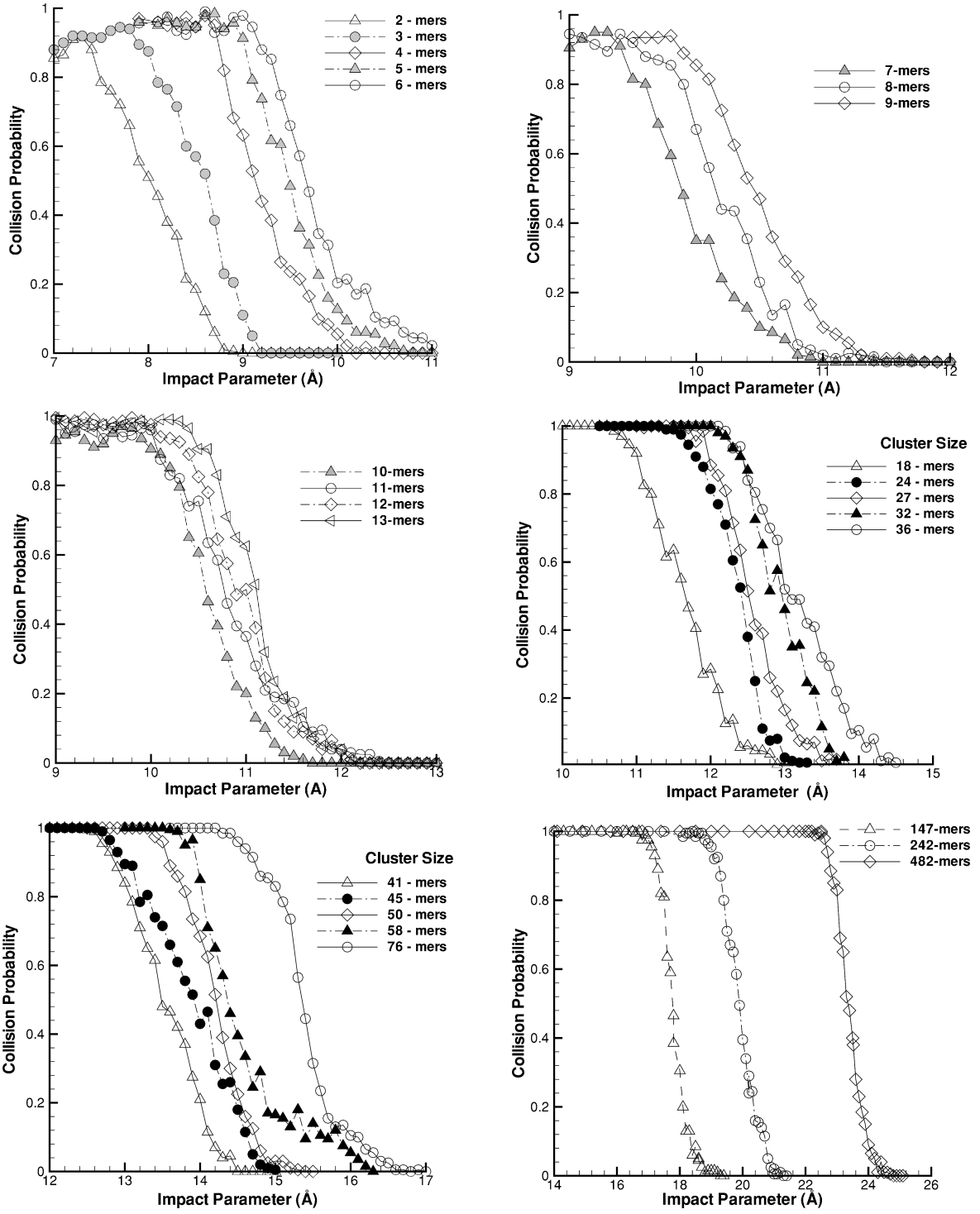

Fig. 1 Comparison of collision probability for some clusters from dimer to 482-mer under the condition of various impact parameters, with a relative collision velocity of 182 m/s.

where d_c and d_0 are the cluster and molecule diameters, respectively. Thus, the cluster radius, $r_i = d_c/2$, can be determined from the MD simulation results, because the monomer diameter is known. The MD results are shown in Fig. 2 with a relative collision velocity of 182 m/s and are fitted to an analytic general cluster-radius equation[22]:

$$r_i = Ai^{\frac{1}{3}} + B \tag{3}$$

where i is the number of molecules in the cluster, and A and B are constants. The MD simulation results for argon clusters fit this equation quite well, as seen by choosing A 2.3 Å and B 3.4 Å (dashed line in Fig. 2).

The MD simulations also show that cluster–monomer collision probabilities are a function of the relative collision velocities. Results of collision probabilities for different cluster sizes and relative cluster–monomer velocities are shown in Fig. 3. It can be seen that the critical impact parameter increases as the relative collision velocity decreases, and therefore, the cluster cross section would also increase as the relative velocity decreases. To model the dependence of cluster diameter on the relative collision velocity c_r, we borrow the following relationship from the VHS[7] model:

$$d = d_{\text{ref}}(c_{\text{ref}}/c_r)^{\nu} \tag{4}$$

where the subscript ref refers to a reference value and ν is a constant related to species viscosity. The MD results for cluster radii,

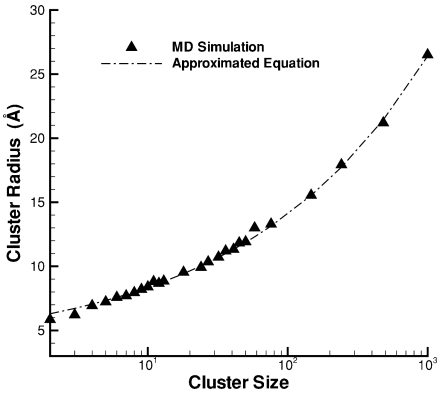

Fig. 2 Average cluster radius from MD simulations with a relative collision velocity of 182 m/s is fitted to an approximated equation, $R_i = 2.3i^{1/3} + 3.4$.

calculated for various relative collision velocities, are shown in Fig. 4 as symbols, and the simulation results fitted to Eq. (4) are shown as dashed lines. For each cluster-size case we choose one of the four MD simulated points as a reference diameter d_{ref} and a reference velocity c_{ref}. Then, we vary the value of ν such that we obtain a smooth fit through all four points. The reference cluster diameter d_{ref} is consistent with Eq. (3). For larger cluster sizes, the value of d_{ref} is higher so that a smaller ν is required to model the cluster-collision-diameter dependence on the relative collision velocity. It can be seen from Fig. 4 that as the cluster size increases from dimer to 147-mer, the best-fit constant ν decreases approximately from 0.3 to 0.07. Note that for argon vapor, the constant ν is about 0.31. Thus, the impact of collision relative velocity on the cluster cross section becomes less as the cluster size increases, which indicates that the HS model may be used to model relatively large clusters in the DSMC simulation. As Fig. 4 shows, the error in using the HS model increases for small clusters.

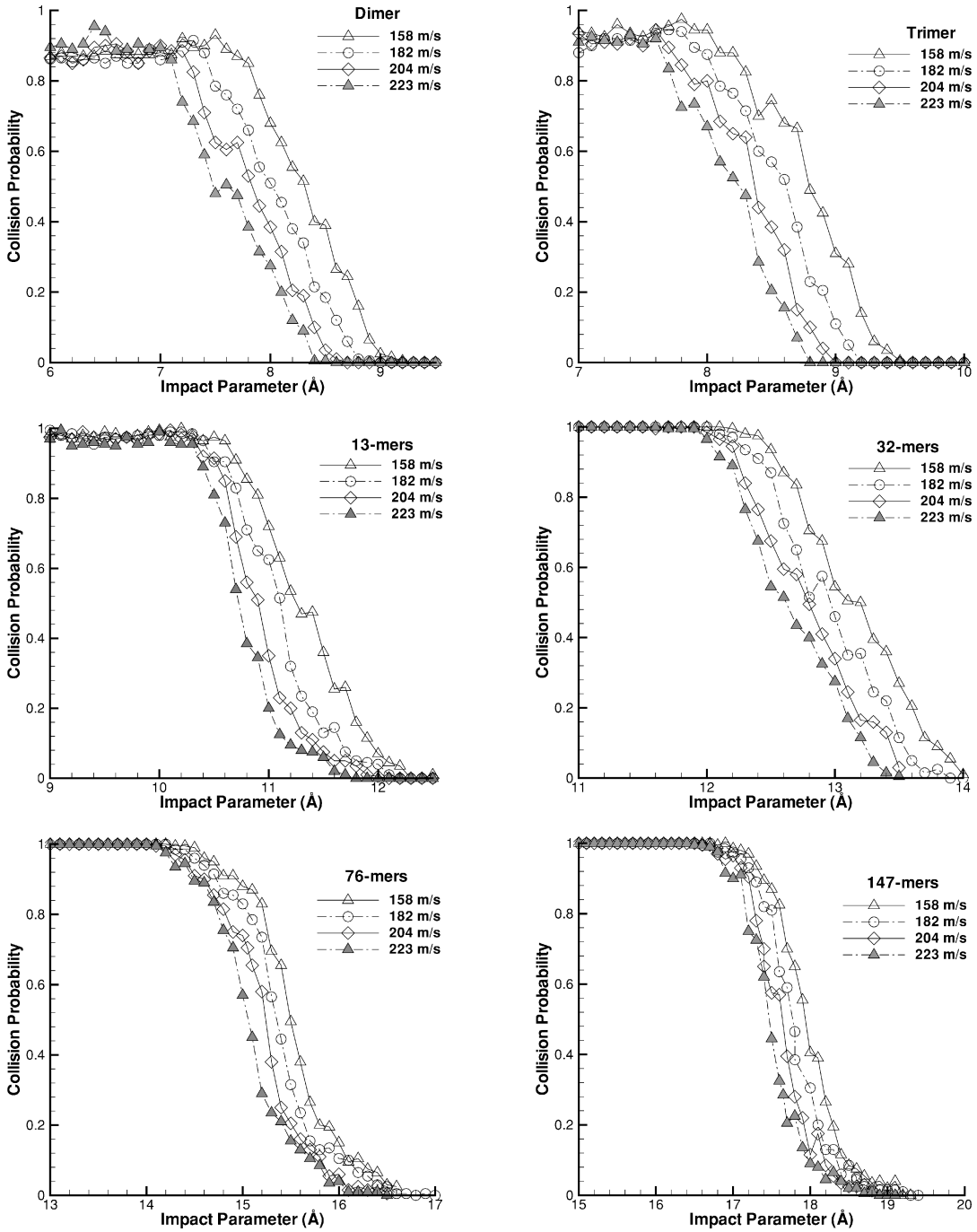

Fig. 3 Comparison of collision probability for some clusters under the condition of various impact parameters and relative collision velocities.

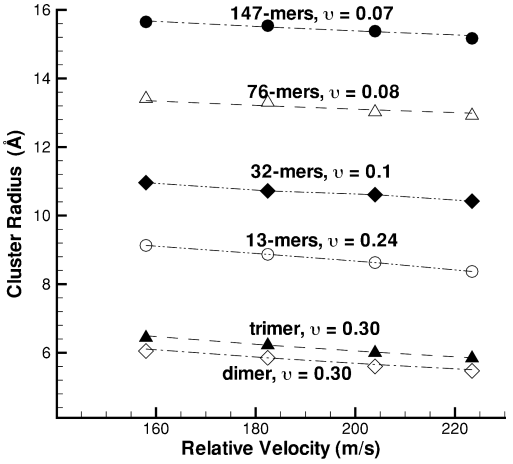

Fig. 4 Cluster radius shown as symbols from MD are fitted to the equation $r = r_{\mathrm{ref}}(c_{\mathrm{ref}}/c_r)^{\nu}$ by choosing one best-fit constant ν.

D. Sticking Collision Probability

The sticking probability for a collision process between a cluster and a molecule can be simulated in a manner similar to the collision probability. Initially, the target argon cluster is at the origin in a static state, while the colliding argon atom is approximately 50 Å away from the cluster. (A static state indicates that the cluster center of mass has no translational velocity and only has thermal motion or internal energy.) It takes about 25 ps before the atom collides with the target cluster. The simulation time for a colliding case is approximately 100 ps, which is also long enough to observe whether the outcome is a sticking or nonsticking collision. To get good statistics, we perform 2500 trajectories for each colliding case by randomly rotating the target cluster, as discussed in Sec. II.C.

It can be expected that cluster–monomer sticking probability is also dependent on the relative collision velocity, especially for small clusters. Similar to the collision probability, the impact of the relative velocity on the sticking probability decreases as the cluster size increases. Figure 5 shows the MD simulation results of sticking probabilities for various cluster sizes and relative velocities as

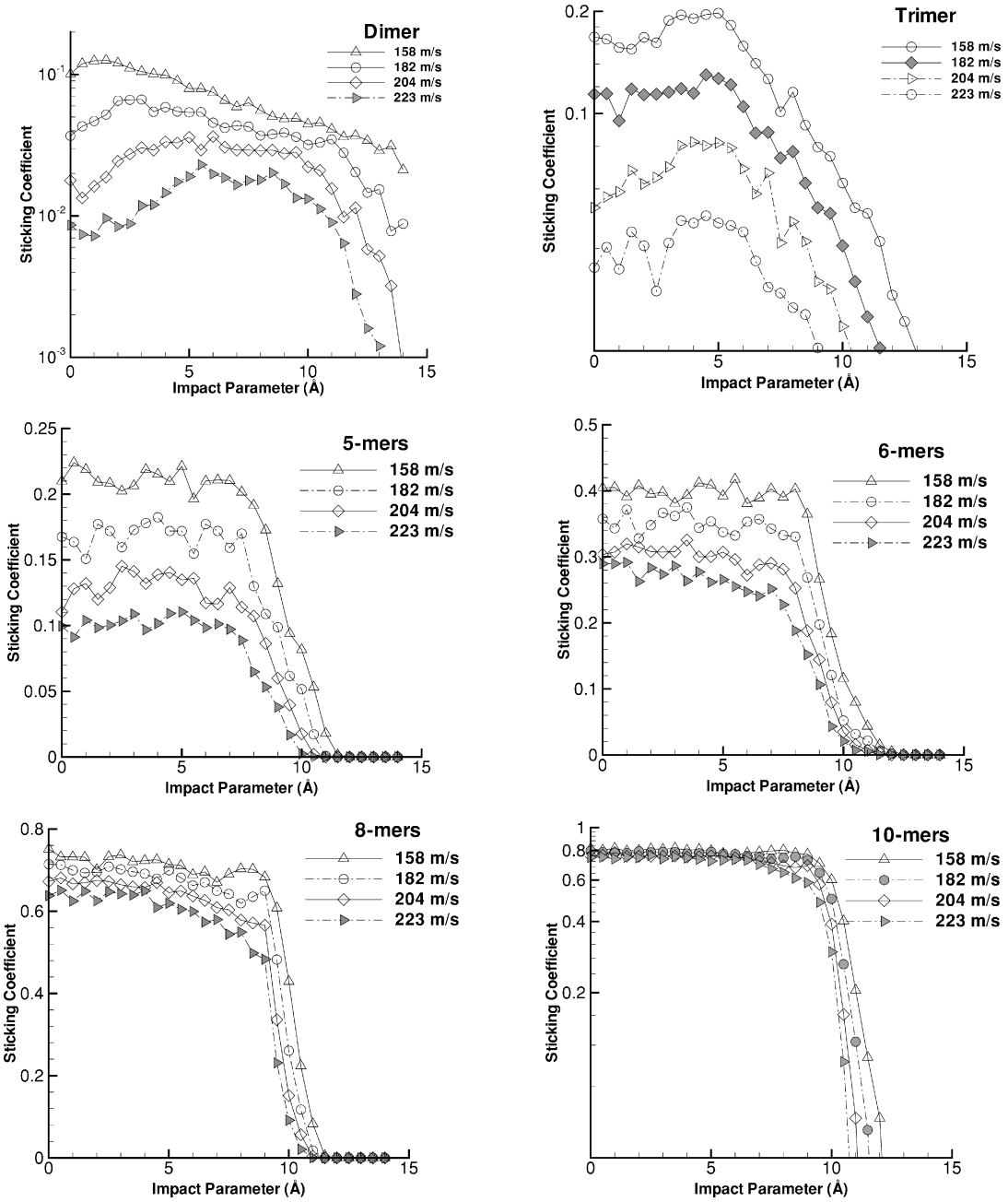

Fig. 5 MD simulation results of sticking-collision coefficient or probabilities for some clusters under the condition, of various impact parameters and relative collision velocities.

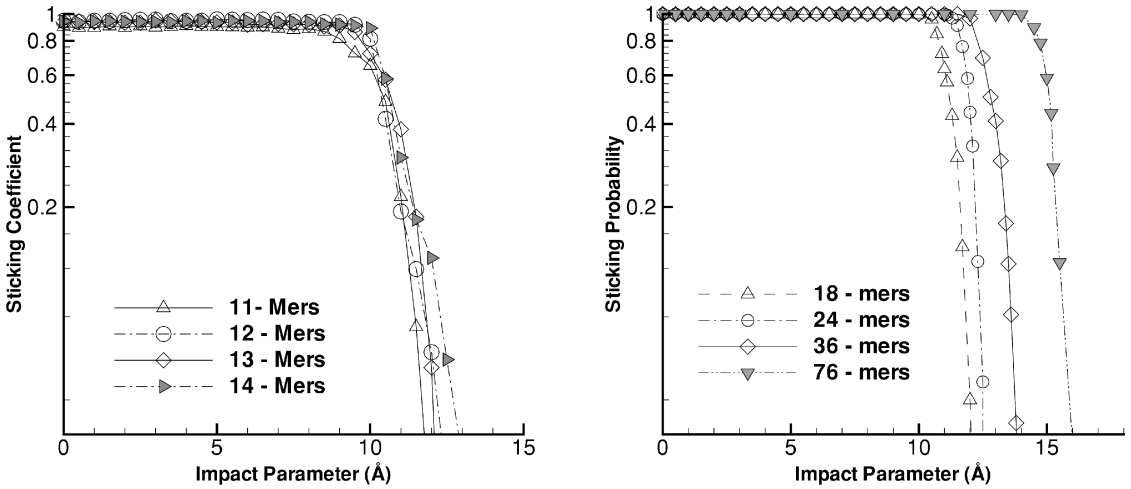

Fig. 6 MD simulation results of sticking collision coefficient for clusters of different sizes as a function of impact parameter, with a relative collision velocity of 182 m/s.

a function of impact parameter. This figure indicates that the sensitivity of the sticking probability to relative velocity decreases as the cluster size increases, and it may be neglected for clusters larger than 10-mers with good approximation. To highlight the size dependence of the sticking probability, Fig. 6 shows the sticking probability as a function of impact parameter for different-size clusters all with a relative collision velocity of 182 m/s. It can be seen that the sticking-collision probability, similar to the collision probability, is critically dependent on impact parameters. For collisions with impact parameters less than the critical impact parameter, the sticking probabilities are almost constant and are unity for cluster sizes of 11-mers and larger. In contrast, for collisions with impact parameters larger than the critical impact parameter, the sticking probabilities decrease to zero even faster than the collision probabilities compared with Fig. 1. As can be seen from Fig. 6, the critical collision impact parameter for the sticking-collision probability increases as the cluster size increases.

In the DSMC simulation of an expanding flow, consisting of gas and clusters, each collision is not modeled in detail and only average collision properties are used. For this reason, the dependence of the sticking probability on impact parameter must be averaged over the collision cross section. The average sticking probability $P^i_{\rm av}$, can be calculated from the MD results for each cluster based on a b^2 distribution of collision pairs,

$$P^i_{\rm av} = \frac{1}{b^2_{i,m}} \int_0^{b_{i,m}} P(b) db^2 \tag{5}$$

where $b_{i,m}$ is the cluster maximum impact parameter or collision radius, given by Eq. (2). Figure 7 shows the averaged sticking probability $P^i_{\rm av}$ as a function of cluster size for a relative collision velocity of 182 m/s. It can be seen that for cluster size smaller than 10, the sticking-collision probability increases quickly as the cluster size increases, whereas for cluster size larger than 10, the sticking-collision probability is independent of cluster size and is very close to unity.

Therefore, the MD simulation results show that for clusters larger than 10-mers, cluster–monomer interactions may be modeled approximately with the HS model, with a constant sticking coefficient of unity. The MD simulation study confirms the selection of these models utilized in the earlier work.[8]

E. Comparison of MD Results for Different Lennard–Jones Systems

Collision processes between argon clusters and molecules have been simulated in the previous sections, and the important results that give cluster size and sticking coefficients are shown in Fig. 2 and Fig. 7 respectively. Because Lennard–Jones potential is generally used to describe molecular interaction for many other gases, the simulated results for argon may be applicable to other species,

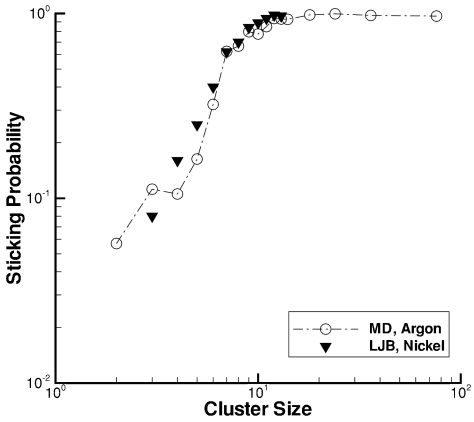

Fig. 7 Average cluster sticking probabilities, for argon clusters from dimer to 76-mer with a relative collision velocity at 182 m/s, are indicated by open circles. Nickel-cluster sticking probabilities are solid symbols.

thereby removing the need to repeat similar MD simulations using the Lennard–Jones parameters specific to the particular gas species. To validate our MD simulations and assess the transferability of our results to other Lennard–Jones systems, we compare our numerical results with other independent data.[14]

Nickel-cluster collision cross sections and sticking-collision process has been simulated by the MD method in the Ref. 14, using a Lennard–Jones potential. First we may directly compare nickel- and argon-cluster sticking probabilities, because the comparison involves a nondimensional parameter. Note that the nickel-cluster sticking probability is defined as the ratio of the cluster sticking cross section to the total cross section, and both quantities are given in Ref. 23. The comparison of argon- and nickel-cluster sticking probability is shown in Fig. 7, represented by open circles and solid triangles respectively. Figure 7 suggests that the trends for small cluster sticking probability discussed in Sec. II.D is similar for both argon and nickel clusters.

To compare cluster collision cross sections for different species, we have to use reduced units to analyze the MD simulation results of Ref. 23. We assume that the cluster cross-sectional radius can be expressed as

$$r_i + r_1 \propto \sigma f(\epsilon, m) \propto \sigma(\epsilon^p / m^q) \tag{6}$$

where r_i is the radius of a cluster consisting of i monomers, r_1 is the monomer's radius, σ and ϵ are the Lennard–Jones parameters, m is the molecular mass, and p and q are constants.

The nickel-cluster cross sections are simulated in Ref. 14 with two Lennard–Jones potentials, the bulk-fitted (LJB) and dimer-fitted

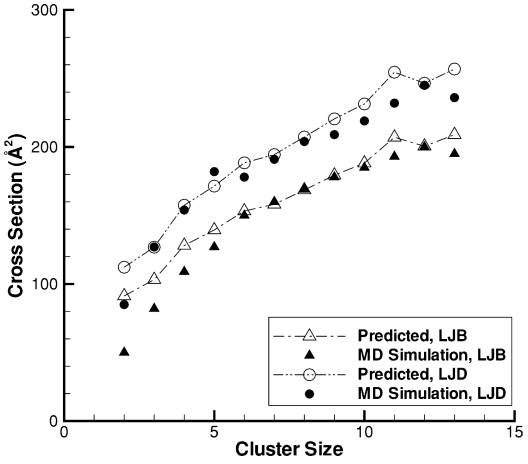

Fig. 8 Comparison of predicted nickel-cluster cross section from simulated argon clusters using Eq. (6) with MD simulation results.

(LJD) potentials. The simulation results for clusters of size from dimer to 13-mers are given in Ref. 14; for example, a 12-mer cluster cross section is about 250 Å^2 for the LJB potential and 200 Å^2 for the LJD potential. The constant p in Eq. (6) can be estimated by comparing these two simulated 12-mer cross sections and was found to be approximately 0.18. Examination of Fig. 2 shows that the 12-mer argon cluster cross section is approximately 363 Å,^{2} which, compared with the nickel cluster computed with the LJB potential, allows one to estimate a q value of approximately 1.56.

By using Eq. (6), the argon-cluster collision cross sections can be used to predict nickel-cluster collision cross sections. A comparison of the argon derived predicted nickel-cross sections, with those obtained in Ref. 14 shown in Fig. 8. It can be seen that the argon cross sections calculated in this work can predict nickel-cluster cross sections well for both nickel interaction potentials. Thus, the argon-cluster sticking probability and collision cross section are consistent with those of nickel clusters, and these results may be extended in the future to approximately estimate other species described by the Lennard–Jones potential.

III. Microscopic Models

Based on general momentum- and energy-conservation concepts, the microscopic models developed have been integrated into a DSMC computational scheme to predict homogeneous condensation in a rocket plume. Detailed descriptions of these models can be found in the previous work.[8] We briefly review these models and the improvements to them compared to our previous work,[8] because they are used in Sec. IV to model condensation in an argon free-expanding plume.

A. Simulated Molecular Models

To simulate condensation coupled flow, all species including monomers and clusters are represented by simulated molecules in the DSMC approach. The VHS model is used to model simulated molecules representing real atoms or molecules in the plume, and the Larsen–Borgnakke model is used to redistribute molecule–molecule collision energy based on the number of degrees of freedom. Note that both rotation- and vibration-energy transfer are considered in molecule–molecule collisions.

An analytic cluster HS model is described in Ref. 22, providing a general asymptotical equation for cluster radius similar to Eq. (3). Briehl and Urbassek[11] applied this cluster model to simulate small copper-cluster growth and decay processes using the DSMC approach. This cluster model has been validated by our MD simulations for argon clusters, discussed in Sec. II.B. It was further shown that the argon-cluster model is consistent with other independent studies of nickel clusters[14] in Sec. II.E. Thus, we use the HS cluster model in our DSMC simulation.

B. Nucleation and Evaporation Models

Following CNT theory,[1] initial clusters, called nuclei, are introduced into the computational domain. The nuclei have the same size as the local critical clusters, and they are in an equilibrium state with the surrounding gas. The nucleation rate J is given in the CNT theory as

$$J = \left(\frac{2\sigma}{\pi m^3}\right)^{\frac{1}{2}} \frac{\rho_v^2}{\rho_c} \exp\left(-\frac{4\pi r_*^2 \sigma}{3k_B T}\right) \tag{7}$$

where σ is the cluster surface tension, m is molecular mass, ρ_v is vapor density, ρ_c is cluster density, and r_* is the local critical cluster radius. Thus, during a time step Δt in a cell with volume ΔV, the number of new simulated nuclei n_c is calculated as

$$n_c = J_c \Delta V \Delta t / F_c \tag{8}$$

where F_c is the number of real molecules represented by a simulated cluster molecule. The latent heat, generated during the nucleation process, is evenly distributed to each degree of freedom of the ambient gas molecules in a cell. Using bulk theory, the latent heat E_L is given by

$$E_L = LM_i \tag{9}$$

where L is the specific latent heat and M_i is the mass of a cluster consisting of i monomers. Because CNT assumes that the clusters have properties of the bulk material, we characterize the internal energy of a cluster in terms of the specific heat capacity of the bulk material c_p as

$$E_{\text{int}} = c_p M_i T_c \tag{10}$$

where i is the number of molecules in the cluster; T_c is the cluster temperature, which initially is assumed to be the local gas translation temperature; and M_i is the cluster mass. The cluster evaporation rate E is given in the CNT theory as

$$E = \frac{4\pi p_s r_c^2}{(2\pi m k T_c)^{0.5}} \exp\left(\frac{2\sigma}{\rho R T_c r_c}\right) \tag{11}$$

where p_s is the vapor saturation pressure and R is the ideal vapor constant. In the evaporation process, the evaporated monomers gain translational and internal energy, reducing the internal energy of the original cluster. The details of computational method of the nucleation and evaporation models are given in Ref. 8.

C. Collision Models

The collision process between a cluster and a foreign molecule is referred to as a nonsticking collision, whereas the outcome of a collision between a cluster and its own molecule may be sticking or nonsticking depending on the sticking-collision probability. Based on MD simulations, a general expression for argon homogeneous sticking coefficient q has been summarized as[24]

$$q = \left(1 - 3\sqrt{V_l/V_g}\right) \exp(-E_o/k_B T) \tag{12}$$

where V_v and V_l are the specific volumes of gas and liquid and E_0 is the energy difference of the minimum quantum level between the activated complex and gas. Equation (12) shows that sticking coefficient is close to unity in the low-temperature region and decreases as the temperature increases. As shown in our MD simulations, sticking coefficients for clusters smaller than 11-mers may not agree with the prediction of Eq. (12) because it is based on the condition of a flat liquid surface. The impact of correctly modeling the sticking probability of clusters smaller than 11-mers on the condensation results is discussed in Sec. IV.

In the previous work, cluster–cluster collisions are assumed to be elastic collisions, without considering the coalescence effect. In this work, the semiempirical Ashgriz–Poo model[25] is chosen to predict the outcome of cluster–cluster collisions that may lead to coalescence or separation. The Weber number, defined as the

ratio of collision kinetic energy to droplet surface energy, provides a cluster–cluster collision separation–coalescence boundary. The Weber number We is given by

$$We = \rho_c d_i c_r^2 \big/ \sigma_c \tag{13}$$

where ρ_c is the cluster density, d_i is the diameter of the smaller cluster, c_r is the cluster–cluster relative velocity, and σ_c is the cluster surface tension. The Ashgriz–Poo model has been verified for droplets by MD simulations using a 6–12 Lennard–Jones potential and was used to predict the outcome of droplet collisions in an inductively coupled plasma.[26] A detailed description of the Ashgriz–Poo model can be found in Ref. 25.

IV. Results and Discussion

The MD simulation results, cluster-collision cross sections and cluster–monomer sticking coefficients, will be integrated into the DSMC simulations. To understand the impact of these improvements and to check the simulation results presented in the previous work,[8] we first compare the improved DSMC simulation results with previous results.

A free argon expanding flow through a sonic nozzle with a convergent angle of 30 deg into a vacuum environment was simulated in Ref. 8. The plume has a stagnation pressure of 5.30×10^4 Pa and a stagnation temperature of 180 K. The DSMC simulation parameters and techniques for this case were described in detail in Ref. 8 and we briefly discuss the important ones here. The two-dimensional axisymmetric simulation domain extends 2 and 10 times the nozzle diameter, 7.0×10^{-4} m, in the radial and axial directions, with 50 and 250 cells, respectively. Using an adaptive grid technique, each cell can be divided into up to 10 subcells according to the flow gradients obtained during the simulation. The number of cells was found to increase from 12,500 to 112,000, and a time step of 1.0×10^{-8} s was used in the DSMC simulation. The number of real molecules represented by a simulated particle, F_{num}, is 5.0×10^7 in the simulations. A single value of F_{num}, 2.5×10^3, is chosen for the cluster species in the simulation because of the several orders of magnitude difference in the cluster and vapor number density. About 2,800,000 simulated molecules are used to represent clusters and vapor molecules at steady state.

Comparisons between improved (new) and previous results (old) are shown in Fig. 9. Because the MD-corrected cluster–monomer collision cross sections are larger than the previous ones, the comparison of average cluster size, shown in the top of the figure, suggests that the cluster size obtained by the improved model is larger than the previous size. However, after the cluster size is normalized to the corresponding terminal cluster size, the middle figure of Fig. 9 shows that the normalized curves of the improved and previous models are almost the same. Note that the terminal cluster size is defined as the average cluster size at the axial position of 20 times the nozzle-throat radius from the nozzle exit. At this location, the cluster-growth process is almost completed because of the lower vapor environment. The middle figure suggests that the improved model still validates the scaling laws of Hagena and Obert,[4] as was shown in the previous work.[8] Finally, the cluster-number densities are compared in the bottom of Fig. 9 and the results suggest that the cluster-number density obtained by the improved model is slightly less than the previous value. The main reason for the decreased cluster-number density in the new results is due to the lower sticking coefficients. This means that the smaller clusters tend to evaporate sooner into separate atoms.

Next, the improved condensation model is applied to a new expanding condensation plume experimentally studied in the Arnold Engineering Development Center (AEDC) in the 1970s.[15] Extensive sets of Rayleigh scattering-intensity data were measured, which may be directly compared with numerical results. A brief summary of the scattering intensity is given here and detailed information can be found in Ref. 15.

Assuming that the condensing flowfield is composed of a collection of gasphase monomers and i-mers with the respective number density N_i and polarizability α_i, the ratio of scattered intensity I_s to

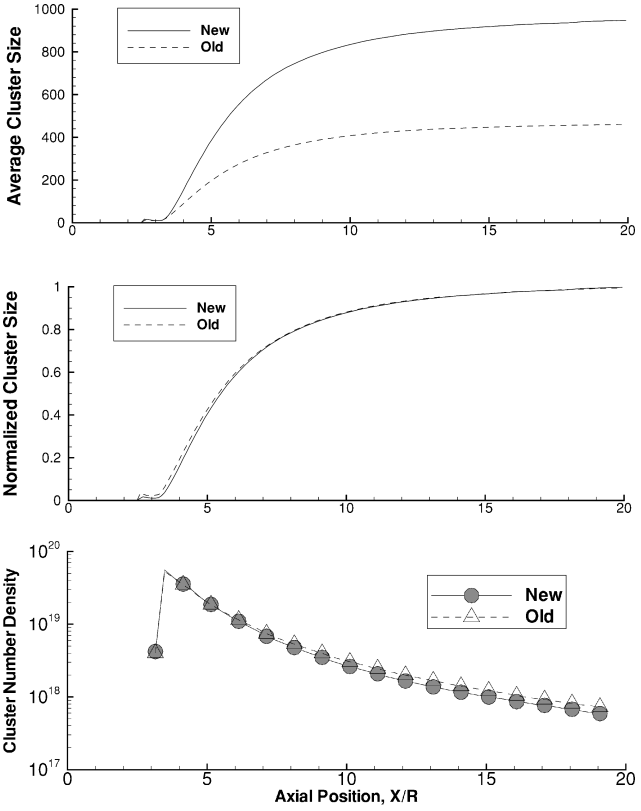

Fig. 9 Contours of argon-cluster size (top), normalized cluster size (middle), and cluster-number density (bottom) along the plume centerline between the improved (new) and previous (old) results. Number density is given per cubic meter. Axial position is normalized to the nozzle throat radius R.

the incident intensity I_0 is given by

$$I_s/I_0 = \sum K N_i \alpha_i^2 \big/ \lambda_0^4 \tag{14}$$

where K is a coefficient containing transmission and calibration factors and λ_0 is the wavelength. Note that polarizability α_i for i-mers is assumed to be i times larger than molecular polarizability α_1.[15]

Here we use the DSMC method to simulate condensation in a free-expanding pure argon plume through a sonic orifice, which had been done experimentally in AEDC[15] with a stagnation pressure of 250 torr, stagnation temperature of 280 K, and orifice diameter of 3.2 mm. The details of DSMC simulation models and techniques are developed in Ref. 8, which can be briefly summarized as follows. The original two-dimensional axisymmetric statisical modeling in low-density environment (SMILE) code[27] is modified to simulate nucleation, cluster–molecule and cluster–cluster collision, and evaporation processes. The simulation domain extends 4 and 10 times the orifice diameter in the radial and axial directions, with 100 and 250 cells, respectively. Each cell can be divided into up to 16 subcells, causing the number of cells to increase from 25,000 to 318,000 during the simulation, and a time step of 2.0×10^{-9} s was used. To decrease the computational cost, radial weights are used for distributing the number of simulated molecules evenly in the radial direction for monomers and clusters. A vapor particle in the simulation represents 1.0×10^{10} real vapor molecules, whereas a cluster particle represents 1.0×10^5 real clusters in the DSMC simulation because of the several orders of magnitude difference in the cluster and vapor number density.[8] Because the noncondensation region close to the orifice is too dense to be modeled by DSMC, the simulation begins from a starting surface, which is created with the continuum solver General Aerodynamics Simulation Program (GASP).[28] About 3,200,000 simulated molecules are used to represent clusters and vapor molecules at steady state. A typical

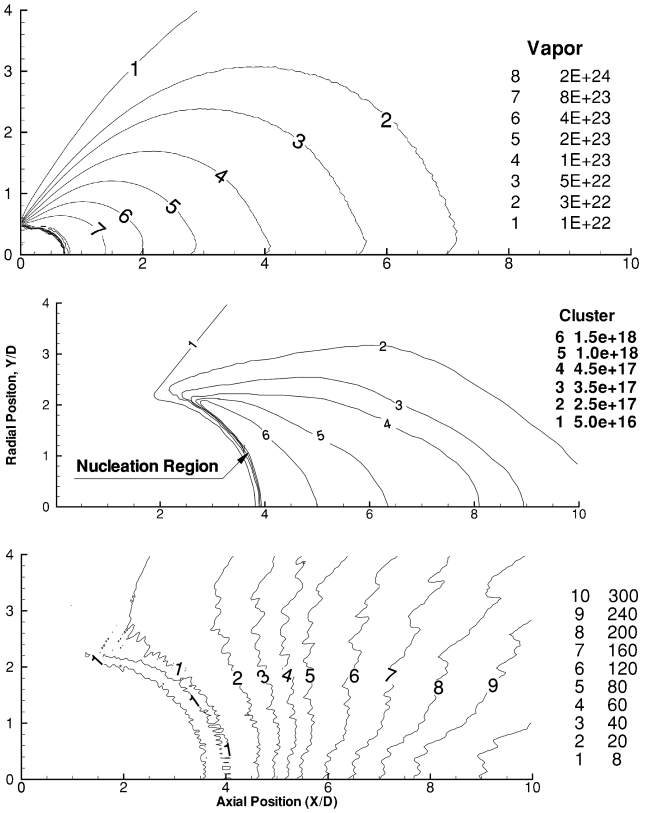

Fig. 10 Contours of argon vapor-number density (top), cluster-number density (middle), and average cluster size (bottom) in the condensation plume, discussed in Sec. IV. Number density is given per cubic meter.

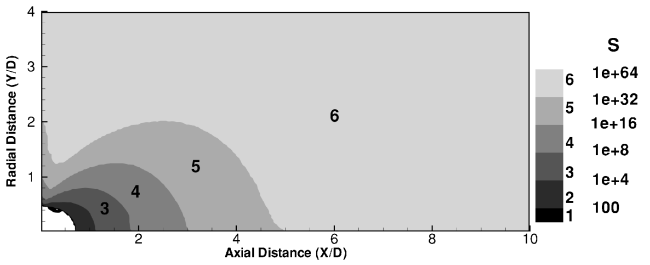

Fig. 11 Distribution of the log of the degree of supersaturation in the free-expanding argon plume.

simulation samples about 400,000 steps and takes 72 hours on 18 parallel AMD Athlon 1526-MHz CPU processors.

The DSMC simulation results for the condensation plume are shown in Fig. 10, including vapor-number-density contours (top), cluster-number-density contours (middle), and average cluster-size contours (bottom). The initial cluster or nuclei appears in a nucleation region where cluster-number density increases quickly along the flow direction consistent with the increased degree of supersaturation during the expanding process, as shown in Fig. 11. Upstream of this region, the gas is essentially an expanding plume without condensation. Further downstream of the nucleation region, cluster-number density decreases mainly because of the expansion. Because the cluster-number density is only on the order of 10^{17} per cubic meter, there are few cluster–cluster collisions and so the importance of the coalescence process on the cluster-number density is limited. The average cluster size is usually below 10-mers in the nucleation region, whereas it increases downstream of the nucleation region because of the sticking collision process between cluster and vapor molecules and cluster evaporation processes. The simulation results were found to be the same with and without inclusion of the Ashrigz–Poo coalescence model.

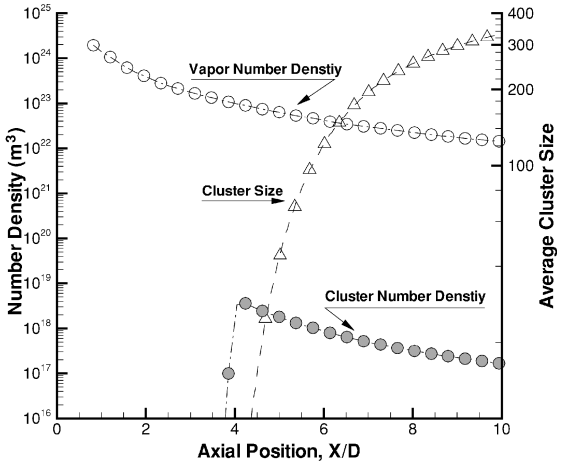

Fig. 12 Distribution of argon gas and cluster-number density, and average cluster size along the centerline of the condensation plume, discussed in Sec. IV.

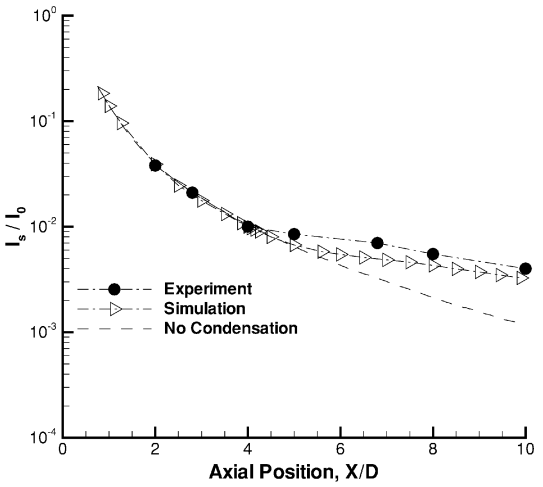

Fig. 13 Comparison of Rayleigh scattering intensity between experimental data and simulation results along the plume centerline. The dashed line indicates intensity of a flow solution without condensation.

The distributions of average cluster size and cluster- and vapor-number density along the core flow are shown in Fig. 12. The figure shows that the vapor-number density is about five orders of magnitude greater than the cluster-number density, whereas the average maximum cluster size in the computational domain is about 300-mers. The average cluster size grows continuously beyond the computational domain until the vapor-number density becomes so low that the contribution of sticking collisions to cluster-growth process counteracts the cluster-evaporation effect.

The Rayleigh scattering intensity is calculated for the flow using Eq. (14), and the core flow is compared with experimental data in Fig. 13. To illustrate the importance of the condensation modeling, a calculation without condensation was performed. The Rayleigh scattering intensity for that specific case is indicated by a dashed line in Fig. 13. Upstream of the nucleation region, there is no condensation in the plume, which leads to a Rayleigh scattering intensity decrease along the flow direction because of rarefaction. However, the emergence of clusters and the cluster-growth process counteracts the decrease of vapor-number density in the condensation region, leading to a scattering intensity downstream of the nucleation region that is larger than its corresponding value in the noncondensation plume. Figure 13 also shows that our numerical results agree reasonably well with the experimental data, thus suggesting that our DSMC condensation model predicts condensation phenomenon in a free-expanding plume correctly. Note that the appearance of nuclei in the DSMC simulation is delayed by 1.2×10^{-5} s to force the initiation of condensation in the simulation to coincide with the

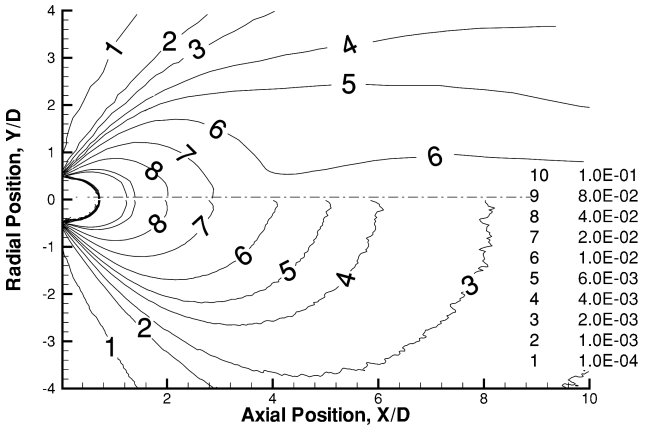

Fig. 14 Comparison of Rayleigh scattering intensity contours I_s/I_0 between condensation (top) and plume without condensation (bottom).

onset of condensation at the position indicated in the experiment. The introduction of this lag time is necessary in this work because we use CNT to model the creation of initial nuclei. In reality there is a finite period of time, known as nucleation lag,[29–31] to build up the nuclei from monomers and to generate a steady-state nucleation rate. The nucleation lag is not important for modeling condensation in a static or low-speed vapor environment; however, it may greatly affect the location where nucleation begins in a high-speed flow. In our case, if we did not introduce a delay, the nuclei in our numerical simulation would appear at a location upstream of the location indicated by the experimental data. For simulation results without a delay time, the cluster size would be larger, and the simulated intensity would not be consistent with the experimental data. This problem is entirely due to the CNT theory because the original formulation of CNT was developed to model static vapor systems such as those in cloud vapor chambers.[32,33]

Figure 14 compares the Rayleigh scattering intensity contours between a condensation (top) and noncondensation (bottom) plume. For the noncondensation case, the plume scattering intensity decreases monotonically in the expanding directions because of the decrease in the vapor-number density. However, for the condensation plume, the scattering intensity decreases more slowly in the axial direction after the initiation of condensation. Consistent with the results shown in Fig. 12, there is a counteracting effect between the increase of the cluster size and the decrease of the cluster-number density. Our numerical simulation results show that there would be a long tail in the Rayleigh scattering intensity distribution in the free-expansion condensation flow. This conclusion holds for both the present and earlier collision and sticking models, as seen in the middle figure of Fig. 9. The exact spatial distribution should be further validated by future experiments.

V. Summary

The general MD approach is used to verify an analytical cluster model and cluster sticking-collision model. The use of Lennard-Jones potential reduced units shows that MD simulation results of argon clusters agree well with those of nickel clusters done in another independent work, indicating that the MD results in this work may be approximately transferred to other species.

The MD simulation results are applied to the DSMC model, which is developed to simulate homogeneous condensation in a free-expanding argon plume through a sonic orifice. According to the DSMC simulation results, Rayleigh scattering intensity is estimated and compared with the experimental data, suggesting that the condensation model developed in this work may reasonably well predict homogeneous condensation in a free-expanding plume. The Rayleigh scattering contours in a condensation plume are predicted, which may need to be validated by experimental data in the future.

Acknowledgments

The authors express their gratitude to M. S. Ivanov for inspiring this study and to L. V. Zhigilei for providing the computer code. This work was supported by Air Force Office of Scientific Research Grant No. F49620-02-1-0104 administered by Mitat Birkan and Army Research Office Grant No. DAAD19-02-1-0196 administered by David Mann.

References

[1]Abraham, F. F., *Homogeneous Nucleation Theory*, Academic Press, New York, 1974.

[2]Lewis, J. W. L., and Williams, W. D., "Profile of an Anisentropic Nitrogen Nozzle Expansion," *Physics of Fluids*, Vol. 19, No. 7, July 1976, pp. 951–959.

[3]Ivanov, M. S., Markelov, G. N., Gerasimov, Y. I., Krylov, A. N., Michina, L. V., and Sokolov, E. I., "Free-Flight Experiment and Numerical Simulation for Cold Thruster Plume," *Journal of Propulsion and Power*, Vol. 15, No. 3, May–June, 1999, pp. 417–423.

[4]Hagena, O. F., and Obert, W., "Cluster Formation in Expanding Supersonic Jets: Effect of Pressure, Temperature, Nozzle Size, and Test Gas," *Journal of Chemical Physics*, Vol. 56, No. 5, 1972, pp. 1793–1802.

[5]Williams, W. D., and Lewis, J. W. L., "Summary Report for the CONTEST Program at AEDC," AEDC-TR-80-16, Sept. 1980.

[6]Perrel, E. R., Erickson, W. D., and Candler, G. V., "Numerical Simulation of Nonequilibrium Condensation in a Hypersonic Wind Tunnel," *JSME International Journal*, Series B, Vol. 39, No. 2, April–June 1996, pp. 277–283.

[7]Bird, G. A., *Molecular Gas Dynamics and the Direct Simulation of Gas Flows*, Oxford Science Publications, New York, 1994.

[8]Zhong, J., Gimelshein, S. F., Zeifman, M. I., and Levin, D. A., "Direct Simulation Monte Carlo of Homogeneous Condensation in Supersonic Plumes," *AIAA Journal*, Vol. 43, No. 8, 2005, pp. 1784–1796.

[9]Sun, Q., Boyd, I. D., and Tatum, K. E., "Particle Simulation of Gas Expansion and Condensation in Supersonic Jets," AIAA Paper 2004-2587, June 2004.

[10]Zeifman, M. I., Garrison, B. J., and Zhigilei, L. V., "Combined Molecular Dynamics—Direct Simulation Monte Carlo Computational Study of Laser Ablation Plume Evolution," *Journal of Applied Physics*, Vol. 92, No. 4, 2002, pp. 2181–2193.

[11]Briehl, B., and Urbassek, H. M., "Monte Carlo Simulation of Growth and Decay Processes in a Cluster Aggregation Source," *Journal of Cacuum Science & Technology A*, Vol. 17, No. 1, Jan.–Feb. 1999, p. 256.

[12]Tsuruta, T., and Naka, Y., "Effect of Noncondensable Gas on Experimental Condensation Coefficient," *JSME International Journal, Series B: Fluids and Thermal Engineering*, Vol. 46, No. 4, Nov. 2003, pp. 557–562.

[13]Allen, M. P., and Tildesley, D. J., *Computer Simulation of Liquids*, Oxford University Press, Oxford, England, U.K., 1987.

[14]Venkatesh, R., Marlow, W. H., Lucchese, R. R., and Schulte, J., "The Effect of the Nature of the Interaction Potential on Cluster Reaction Rates," *Journal of Chemical Physics*, Vol. 104, No. 22, June 1996, pp. 9016–9026.

[15]Lewis, J. W. L., and Williams, W. D., "Argon Condensation in Free-Jet Expansion," AEDC-TR-74-32, July 1974.

[16]Matyushov, D. V., and Schmid, R., "Calculation of Lennard–Jones Energies of Molecular Fluids," *Journal of Chemical Physics*, Vol. 104, No. 21, June 1996, pp. 8627–8638.

[17]Yasuoka, K., and Matsumoto, M., "Molecular Dynamics of Homogeneous Nucleation in the Vapor Phase. I. Lennard–Jones Fluid," *Journal of Chemical Physics*, Vol. 109, No. 19, 1998, pp. 8451–8463.

[18]Zeifman, M. I., Zhong, J., and Levin, D. A., "A Hybrid MD-DSMC Approach to Direct Simulation of Condensation in Supersonic Jets," AIAA Paper 2004-2586, June 2004.

[19]Zhong, J., Zeifman, M. I., and Levin, D. A., "Direct Simulation of Condensation in a One-Dimensional Unsteady Expansion: Microscopic Mechanisions," *Physics of Fluids* (submitted for publication).

[20]Soto, R., and Cordero, P., "Cluster Birth–Death Processes in a Vapor at Equilibrium," *Journal of Chemical Physics*, Vol. 110, No. 15, April 1999, pp. 7316–7325.

[21]Bernshtein, V., and Oref, I., "Dependence of Collision Lifetimes on Translational Energy," *Journal of Physical Chemistry*, Vol. 105, No. 14, 2001, pp. 3454–3457.

[22]Muller, H., Fritsche, H. G., and Skala, L., "Analytic Cluster Models and Interpolation Formulae for Cluster Properties," *Clusters of Atoms and Molecules I: Theory, Experiment, and Clusters of Atoms*, edited by H. Haberland, Springer-Verlag, 1995, pp. 115–138.

[23]Withers, I. M., "A Computer Simulation Study of Tilted Smectic Mesophases," Ph.D. Dissertation, Materials Research Inst., Sheffield Hallam University, 2000.

[24]Nagayama, G., and Tsuruta, T., "A General Expression for the Condensation Coefficient Based on Transition State Theory and Molecular Dynamics Simulation," *Journal of Chemical Physics*, Vol. 118, No. 3, March 2003, pp. 1392–1399.

[25]Ashgriz, N., and Poo, J. Y., "Coalescence and Separation in Binary Collisions of Liquid Drops," *Journal of Fluid Mechanics*, Vol. 221, Dec. 1990, pp. 183–204.

[26]Benson, C. M., Zhong, J., Gimelshein, S. F., Levin, D. A., and Montaser, A., "Simulation of Droplet Heating and Desolvation in Inductively Coupled Plasma—Part II: Coalescence in the Plasma," *Spectrochimica Acta, Part B: Atomic Spectroscopy*, Vol. 58, No. 8, 2003, pp. 1453–1471.

[27]Ivanov, M. S., Markelov, G. N., and Gimelshein, S. F., "Statistical Simulation of Reactive Rarefied Flows: Numerical Approach and Application," AIAA Paper 98-2669, June 1998.

[28]"The General Aerodynamic Simulation Program, GASP version 4.1, Computational Flow Analysis Software for the Scientist and Engineer, User's Manual," Aerosoft Inc., Blacksburg, VA.

[29]Wu, D. T., "The Time Lag in Nucleation Theory," *Journal of Chemical Physics*, Vol. 97, No. 4, Aug. 1992, pp. 2644–2650.

[30]Wyslouzil, B. E., and Wilemski, G., "Binary Nucleation Kinetics III. Transient Behavior and Time Lags," *Journal of Chemical Physics*, Vol. 103, No. 3, July 1996, pp. 1090–1100.

[31]Zeifman, M. I., Zhong, J., and Levin, D. A., "Applicability of the Homogeneous Nucleation Theory to the Condensation in Unsteady Gas Expansions," *Proceedings of the 24th International Symposium on Rarefied Gas Dynamics*, edited by M. Capitelli, American Inst. of Physics, College Park, MD, 2004, pp. 509–516.

[32]McDonald, J. E., "Homogeneous Nucleation of Vapor Condensation I. Thermodynamic Aspects," *American Journal of Physics*, Vol. 30, No. 12, Dec. 1962, pp. 870–877.

[33]McDonald, J. E., "Homogeneous Nucleation of Vapor Condensation. II. Kinetic Aspects," *Journal of Physics*, Vol. 31, No. 1, Dec. 1963, pp. 31–41.